Bulletin of the Seismological Society of America, Vol. 98, No. 4, pp. 2073–2079, August 2008, doi: 10.1785/0120070215

Short Note

Spectral Discrimination between Quarry Blasts and Earthquakes in Southern California

by Bettina P. Allmann, Peter M. Shearer, and Egill Hauksson

Abstract We compare *P*-wave spectra of quarry blasts and earthquakes recorded by the southern California seismic network (SCSN) between 2000 and 2005, with the goal of developing methods to discriminate between these events. We process the spectra using an iterative robust least-squares method to isolate source, receiver, and propagation path contributions. This corrects for first-order attenuation structure, as well as near-receiver site effects and any errors in the instrument response functions. Using the earthquake spectra and a simple ω^{-2} source model, we compute an empirical Green's function (EGF) to remove the trade-off between the source terms and other parameters in our model. A constant stress-drop model gives a good fit to the observed average earthquake spectra over a wide range of moment magnitude, but provides a mediocre fit to the average quarry blast spectra, which have a generally steeper fall-off at high frequencies than ω^{-2}. We also compare *P*- and *S*-wave amplitudes and find modestly smaller average *S* amplitudes for the explosions compared to the earthquakes. For southern California, the root-mean-square (rms) misfit of *P*-wave spectra to an ω^{-2} source model is a more reliable explosion discriminant than the *S*-to-*P* amplitude ratio and works for about 90% of the events.

Introduction

A challenge in seismic monitoring of a comprehensive nuclear test ban treaty (CTBT) is to uniquely discriminate between natural seismicity and anthropogenic events such as mining blasts. A variety of waveform-based discrimination methods have been developed and investigated over the last five decades (see Stump *et al.*, 2002 for a recent review). These methods can be roughly divided into: (i) determining amplitude ratios between seismic phases (e.g., Bennett and Murphy, 1986; Wuester, 1993; Plafcan *et al.*, 1997; McLaughlin *et al.*, 2004), (ii) spectral methods (e.g., Taylor *et al.*, 1988; Gitterman and van Eck, 1993; Smith, 1993; Walter *et al.*, 1995; Carr and Garbin, 1998; Gitterman *et al.*, 1998; Hedlin, 1998), and (iii) coda studies (e.g., Su *et al.*, 1991; Hartse *et al.*, 1995).

In many regions, quarries are well established and produce frequent explosions that can be identified simply by their locations. In areas where quarry data are incomplete, clusters of seismicity can nonetheless often be flagged as artificial by computing the fraction of events occurring during daylight hours, as quarry blasts occur almost entirely during the daytime (Agnew, 1990; Richards-Dinger and Shearer, 2000; Wiemer and Baer, 2000). Quarry blasts are commonly detonated as distributed charges that are fired with a series of delays in order to control the movement of rock masses during the blast. These so-called ripple-fired explosions can often be discriminated by a characteristic time-invariant spectral modulation that is caused by the time delays between subsequent explosions (Hedlin *et al.*, 1989, 1990; Kim *et al.*, 1994; Arrowsmith *et al.*, 2006, 2007).

Earthquakes, on the other hand, have a different spectral signature that is related to the physics of shear faulting and is theoretically described by source models such as those of Brune (1970) and Madariaga (1976). In this article, we systematically analyze and compare observed source spectra from locally recorded earthquakes and explosions in southern California in order to develop additional criteria for quantitative discrimination methods. We exploit the large numbers of sources and receivers available from the southern California seismic network (SCSN) to isolate the source spectra from propagation path effects, using the spectral stacking method first introduced by Warren and Shearer (2000, 2002). We focus on *P*-wave spectra because we find that they have a good signal-to-noise (STN) ratio over a much wider bandwidth than the *S*-wave spectra, but we also examine some simple measurements of peak *P* and *S* amplitudes.

Data and Method

We use data recorded at three-component high-gain broadband stations of the SCSN between 2000 and 2005 (Fig. 1). We obtain waveforms from an online database stored on a redundant array of inexpensive (or independent) drives system at the California Institute of Technology, which provides complete access to the SCSN seismogram archive (Hauksson and Shearer, 2005). Out of a total of 88,252 events that we used in this study, 4605 are labeled as quarry blasts by the SCSN network. We have verified the accuracy of these identifications by examining day/night maps of seismicity, and in this article, we will assume that the assigned event types are definitive. By using these known events, our goal is to see whether there are differences in the waveforms between earthquakes and explosions that might permit event identification in the case where the event location is not associated with a known quarry. Our spectral processing approach closely follows that of Shearer *et al.* (2006), who conducted a comprehensive analysis of small-magnitude earthquakes in southern California to which we refer the reader for additional details.

We compute displacement spectra over a 1.28-sec window before and after the picked *P*- and *S*-arrival times using a Hanning taper. The *P* and *S* picks and their respective amplitudes are obtained using the operator pick, if available, or using the output of an automatic picking algorithm for a window around the predicted arrival time, which is based on the catalog event location and a one-dimensional (1D) velocity model. The data are sampled at 100 Hz, resulting in a Nyquist frequency of 50 Hz, although the STN ratio deteriorates beyond 20–30 Hz. We require that the average STN ratio for each spectrum exceed 3 within separate frequency bands of 5–10, 10–15, and 15–20 Hz. Each earthquake is required to have at least three different stations that produce records satisfying our STN criteria.

Because we are only interested in source effects, the next step is to isolate the source part of the displacement spectrum from attenuation and other path effects. Each observed displacement spectrum $d_{ij}(f)$ of source i and receiver j is a product of a source term e_i (which includes the source spectrum and near-source attenuation), a near-receiver term s_j (which includes any uncorrected part of the instrument response, the site response, and the near-receiver attenuation), and a travel-time-dependent term $t_k(i, j)$ (which includes the effects of geometrical spreading and attenuation along the ray path). In the log domain, this product becomes a sum,

$$d_{ij} = e_i + s_j + t_{k(i,j)} + r_{ij}, \tag{1}$$

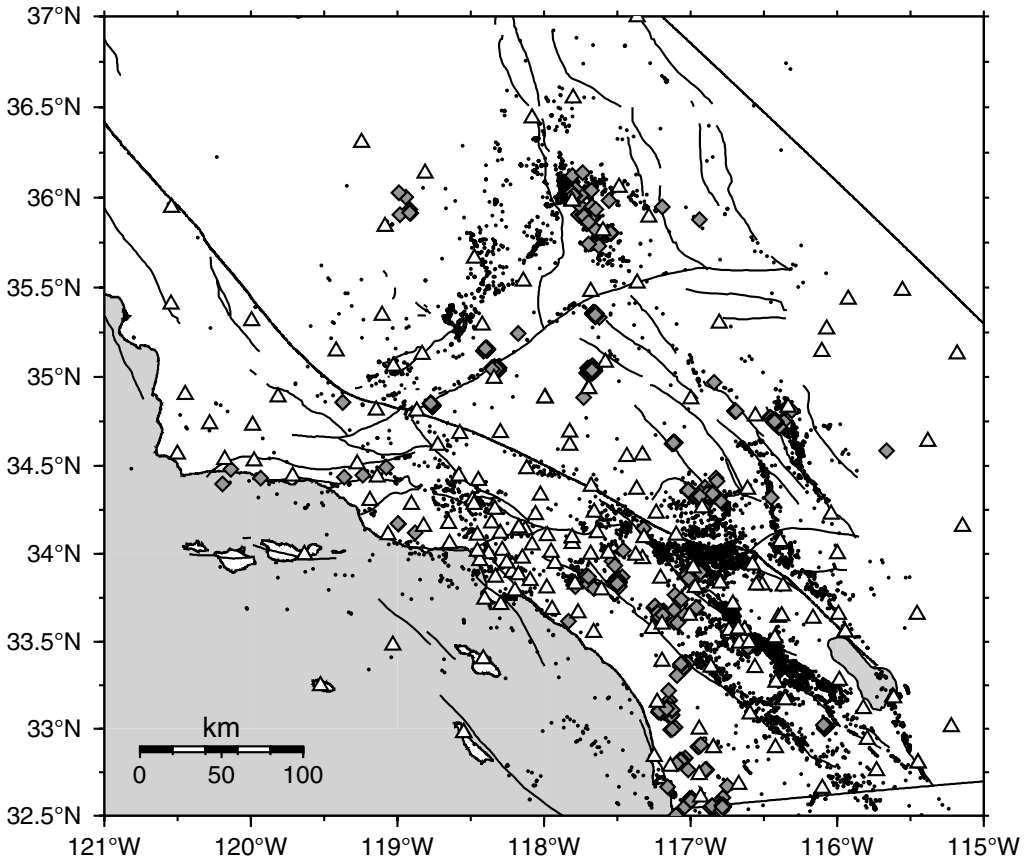

Figure 1. Event and station distribution in southern California. 18,101 earthquakes (black dots) and 1770 quarry blasts (gray diamonds) were used in the analysis recorded at 196 broadband stations (white triangles). Main faults are included as black lines.

where r_{ij} is a residual term. For many local events recorded by an array of stations, equation (1) constitutes an overdetermined problem, which we solve using a robust iterative least-squares approach. Similar to Warren and Shearer (2000, 2002), Prieto *et al.* (2004), and Allmann and Shearer (2007), we sequentially solve for the terms e_i, s_j, and t_k, while keeping the other terms fixed at each stage. The travel-time term $t_{k(i,j)}$ is discretized at increments of 1 sec, where we use the event locations and velocity model from Lin *et al.* (2007).

The source spectra obtained in this fashion contain only relative information among events at this step and need to be corrected to obtain absolute spectra. This is done by tying the relative moment magnitude estimate Ω_0, obtained from the low-frequency part of the spectra, to absolute moment magnitude M_{w} using the local catalog magnitude M_{L} and applying an empirical Green's function (EGF) correction to obtain true spectral shapes. We compute the EGF by stacking earthquake source spectra within 0.2 unit bins of local magnitude and fitting a constant parameter source model to the observed spectral stacks. The best-fitting constant stress drop is 2.15 MPa, based on the ω^{-2} model of Madariaga (1976). The median residual for each frequency point between the source stacks and the predicted model over a local magnitude range from M_{L} 1.5 to M_{L} 2.7 results in the EGF. Figure 2 shows the raw and EGF-corrected source spectral stacks for earthquakes and explosions. Because of the large number of stacked traces, estimated standard errors for the stacks are typically less than 10^{-4} (earthquakes) and 10^{-3} (quarry blasts) in log amplitude, except for the largest and smallest magnitude bins, which have fewer data and standard errors up to 0.04 (earthquakes) and 0.08 (quarry blasts) in log amplitude.

The average earthquake spectra in southern California are well fit by the ω^{-2} source model. However, the average quarry spectra appear anomalous in at least two aspects: (1) they exhibit a large misfit compared to the source model predictions and (2) they have generally steeper fall-offs at high frequencies than ω^{-2}, which will lead to lower-corner frequency estimates. The steeper fall-off rate in the source spectral stacks of quarry blasts is prominent over the whole magnitude range (Fig. 2c). We observe the same behavior also in the unstacked source spectra of individual events, even though individual event spectra are much more scattered. This lower-frequency content of explosions has been observed in previous studies (e.g., Taylor *et al.*, 1988; Su *et al.*, 1991; Gitterman and van Eck, 1993). The relative lack of high frequencies in quarry blasts might reflect ripple firing and/or strong attenuation in the near-surface layers. In some cases, we observe slight spectral modulations at regular distributed frequency intervals in the quarry blast spectra, which can be explained by ripple-fired explosions. However,

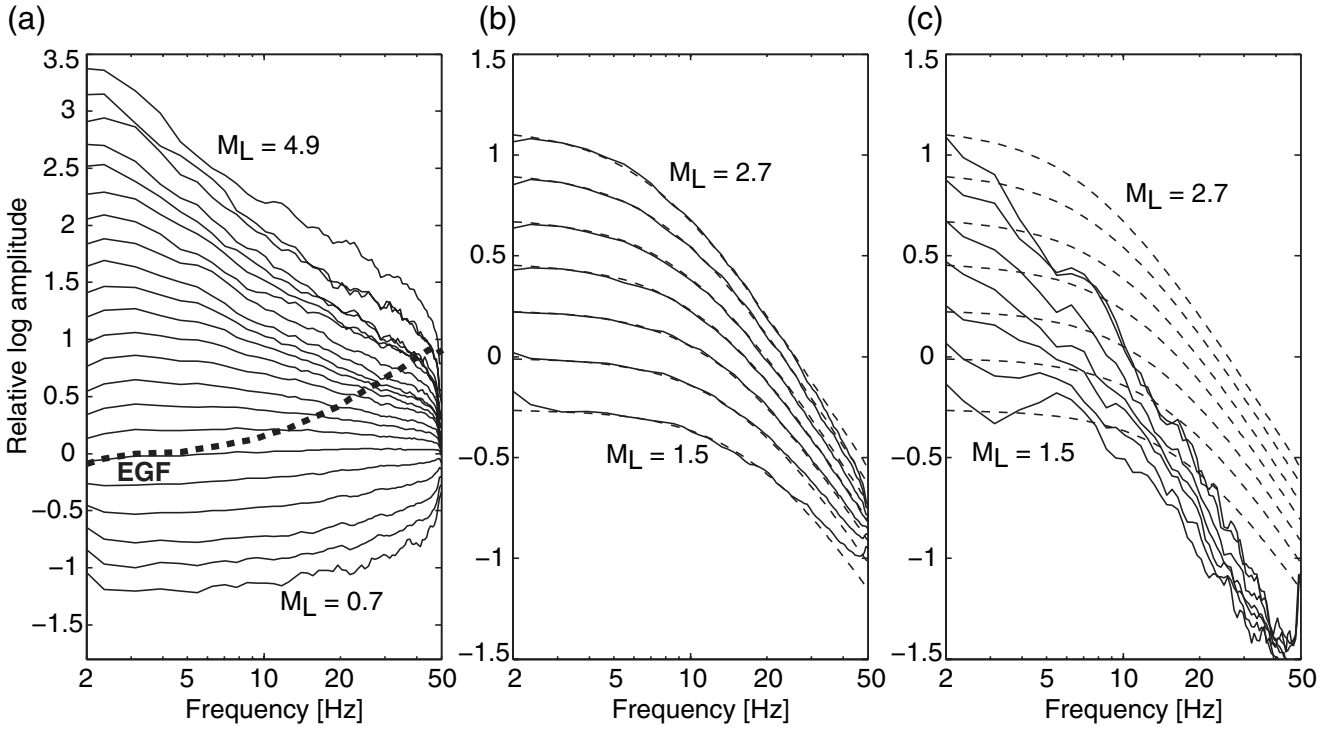

Figure 2. Stacked *P*-wave source displacement spectra within 0.2 unit bins of local magnitude for earthquakes and quarry blasts. (a) Stacked raw earthquake source spectra. The dashed line shows the EGF used to correct these spectra. (b) EGF-corrected earthquake source terms (solid line) in comparison to the best-fitting theoretical model (dashed line). (c) EGF-corrected quarry blast source terms (solid line) compared to the predicted earthquake source model (dashed line).

varying time delays between subsequent sources for different quarries cause incoherent stacking of the spectral modulation.

Figure 3 shows example *P* and *S* waveforms and spectra for earthquakes and quarry blasts at good and fair STN ratios. We observe a reasonable STN ratio up to about 20 Hz for the *P*-wave spectra and only poor STN ratios for most *S*-wave spectra, in large part due to contamination from *P* coda. For this reason, we focus on the *P*-wave spectra from vertical-component data in this study. The waveforms in the displayed examples do not reveal a noticeable difference in *S*-to-*P* amplitude ratios between earthquakes and quarry blasts, although, as we will discuss later, there is a difference in their average amplitude ratio when all of the events are analyzed.

Results

Spectral Properties

Based on these observations, we attempt to use the root-mean-square (rms) misfit to the ω^{-2} source model and the observed corner frequency f_c as discriminants between earthquakes and artificial events. The corner frequency f_c of individual events is estimated from the deconvolved source spectra using a least-squares fit between 2 and 20 Hz. We obtain estimates of seismic moment magnitude, corner fre-

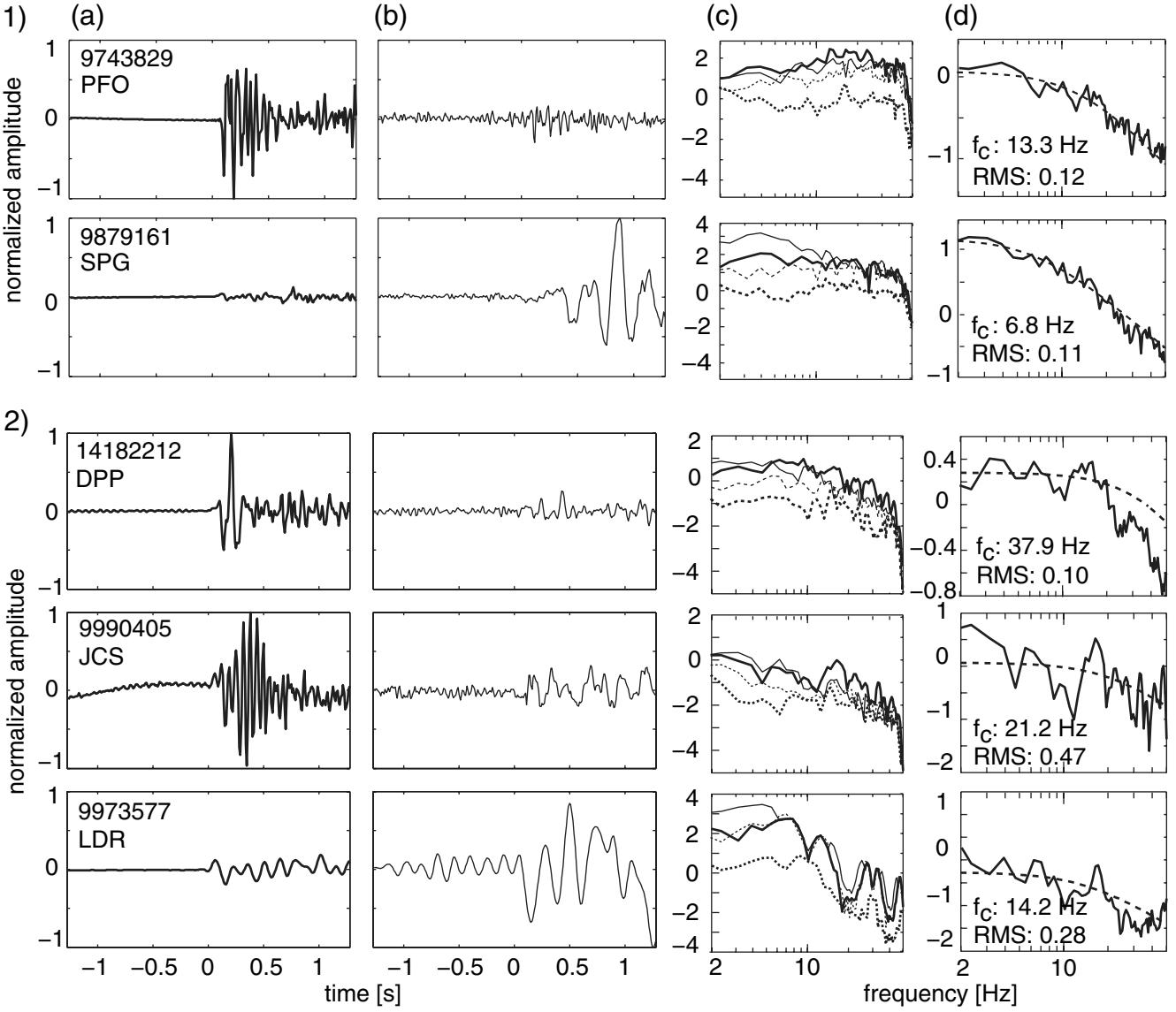

Figure 3. Part (1) shows two examples of earthquake waveforms and spectra. Part (2) shows three examples of quarry blast waveforms and spectra. (a) Waveforms windowed around the *P*-wave first arrival recorded on the vertical component. Event and station identification is included. (b) Waveforms windowed around the *S*-wave arrival recorded on the rotated transverse component of same station. (c) Spectra for *P* (bold black line), *S* (thin black line), and respective noise levels (dashed line). (d) EGF-corrected *P*-wave source spectra (solid line) together with the best-fitting source model (dashed line).

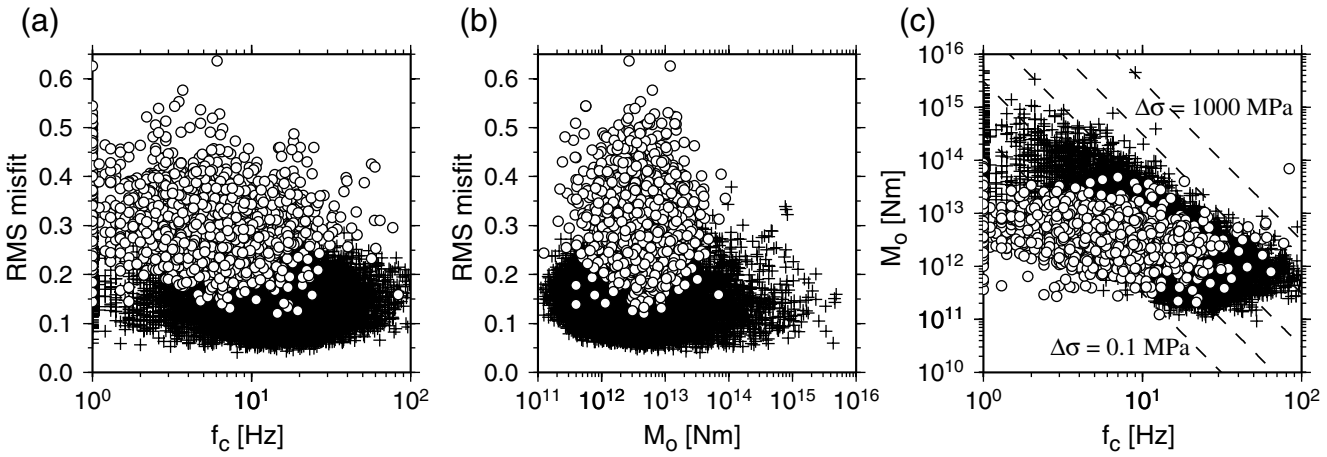

Figure 4. Comparison of earthquakes (black crosses) and quarry blasts (white circles) using various discriminating parameters. (a) rms misfit to an ω^{-2} source model versus corner frequency. (b) rms misfit versus seismic moment magnitude. (c) Seismic moment magnitude versus corner frequency. Dashed lines show constant stress-drop estimates ranging from 0.1 to 1000 MPa from the Madariaga (1976) model.

quency, and rms misfit for 18,101 earthquakes and 1770 quarry blasts. Figure 4 shows comparisons of the rms misfit versus M_0 and f_c for earthquakes and quarry blasts, respectively. Note that we do not observe a dependence of rms misfit on f_c or M_0, which is an indication that the rms misfit might be usable as a discriminant.

In general, the quarry blasts have higher rms misfits and smaller f_c than the earthquakes. However, the two populations are not completely separated and there is some degree of overlap, particularly in the corner frequency estimates. As we would expect, the moment magnitude range is much narrower for quarry blasts than for earthquakes. Figure 4c includes lines of constant stress drop $\Delta\sigma$ estimated from the source model. Although $\Delta\sigma$ is not defined for quarry blasts, we obtain lower stress-drop estimates for explosions compared to earthquakes. The median stress-drop distribution for earthquakes suggests self-similarity, although the scatter significantly increases towards smaller moment magnitude. This is consistent with earlier results from Shearer *et al.* (2006). In order to find out how well the quarry blasts and earthquake populations separate, we show histograms of the rms misfit and f_c in Figures 5 and 6. Our results suggest that a line can be drawn around a rms misfit value of 0.2 below which 90% of all the earthquake misfits are located.

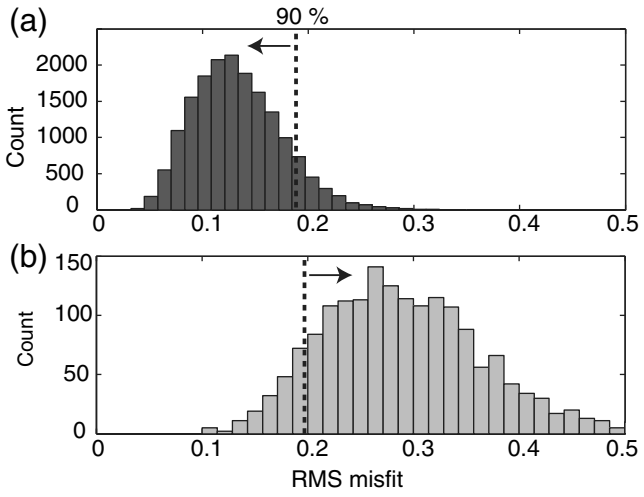

Figure 5. Histograms of rms misfit to an ω^{-2} source model for (a) earthquakes and (b) quarry blasts. Dashed lines show the 90% boundary.

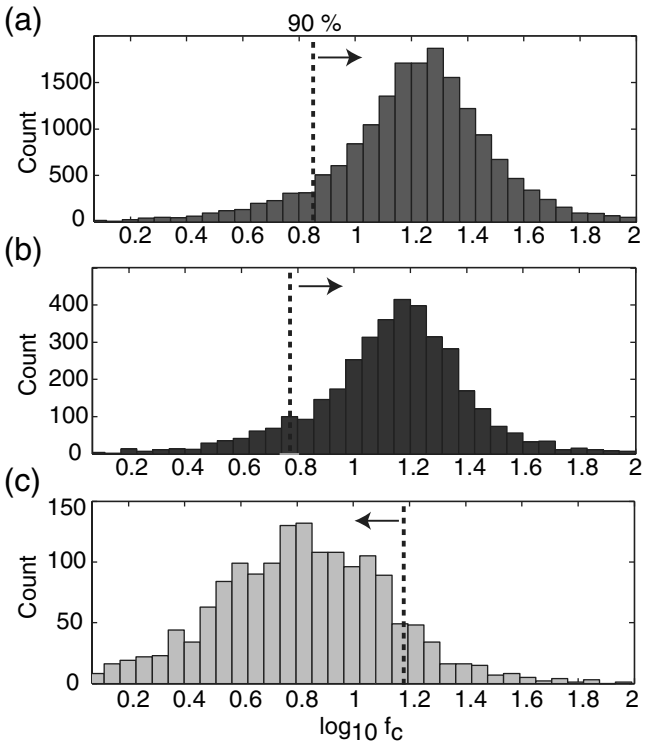

Figure 6. Histograms of corner frequency for (a) earthquakes, (b) shallow earthquakes above 5 km, and (c) quarry blasts. Dashed lines show the 90% boundary.

Above this line, we find 90% of the quarry blast misfits (Fig. 5). Using the corner frequency as a discriminant, we observe a larger region of overlap, and the 10% and 90% quantiles are at significantly different values for earthquakes and quarry blasts (Fig. 6).

In order to rule out the possibility that the lower-corner frequencies for quarry blasts are an effect of higher attenuation near the surface (i.e., near the source), we recalculated the histogram only for earthquakes within the upper 5 km of the crust (Fig. 6, middle). The result is similar and the mean of the histogram is only marginally lower.

Amplitude Ratios

Because a relative lack of radiation is an often-used explosion discriminant, we compare *P*- and *S*-wave amplitudes for earthquakes and quarry blasts using the peak amplitudes in the seismograms, band-pass filtered between 1 to 10 Hz, from the vertical and transverse components, respectively. The underlying idea for this comparison is the preferential excitation of *P* energy relative to *S* energy for explosive sources. We require an STN ratio of at least 3 for all of the *P* waves and compare *P* and *S* peak amplitudes for these events. We observe slightly lower average S/P amplitude ratios for the quarry blasts (Fig. 7), although there is a large amount of overlap in the distributions. The *S* waves for both earthquakes and explosions are often of higher amplitudes than the *P* waves, although we might expect a mean S/P amplitude ratio closer to unity for ripple-fired quarry blasts (Kim *et al.*, 1994). In order to avoid interference of the *P* coda with the *S*-wave first arrival, we also looked only at traces with an epicentral distance greater than 100 km, which significantly reduced the amount of data. The difference in the S/P amplitude ratio between the earthquakes and quarry blasts is larger at these distances, but there is still a significant overlap (Fig. 8).

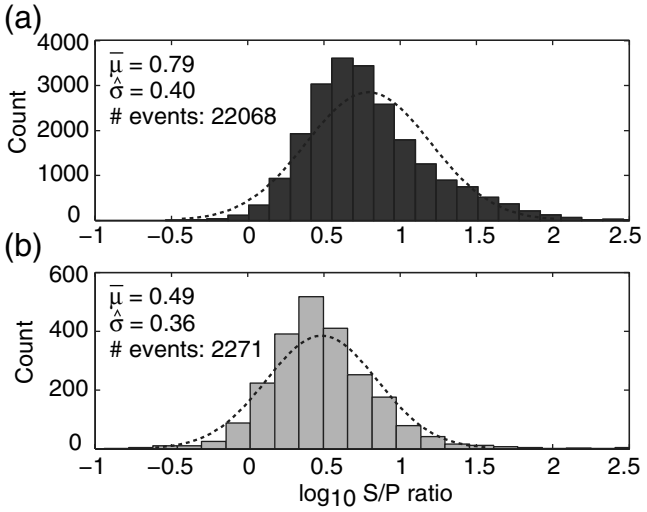

Figure 7. Histograms of S/P amplitude ratios for (a) earthquakes and (b) quarry blasts. The mean $\bar{\mu}$ distribution for quarries is slightly lower with comparable standard deviations $\hat{\sigma}$.

Discussion and Conclusions

The best single waveform discriminant between earthquakes and explosions for locally recorded data in southern California is the rms misfit to an ω^{-2} source model, which works for more than 90% of the events (Fig. 5). Quarry blast spectra are not well fit by standard earthquake source models and exhibit anomalously high spectral fall-off rates compared to earthquakes of the same estimated moment magnitude. However, none of our discriminants were able to completely separate the two populations of events. One might be able to achieve a better separation between the two populations by combining our spectral misfit with a multivariate discrimination approach such as that presented by, for example, Walter *et al.* (1995).

One possible reason for the incomplete separation might be some misclassification of events because the events used in this study were preflagged by the SCSN catalog, based only on event location and the daytime/nighttime distribution. We find an empirical value of 0.2 for the rms source model misfit in log amplitude between 2 and 20 Hz, at which the quarry blast population in southern California generally separates from the natural seismicity. During the investigated time period (2000–2005), we found no spatial correlation of anomalous spectral signatures, as well as no distinct clustering of quarry events within our discrimination plots to explain possible outliers. The S/P amplitude ratio does not reliably separate explosions from locally recorded natural seismicity in southern California. Although our method is based on waveform analysis, it can be carried out automatically using a short window around the *P*- or *S*-arrival time,

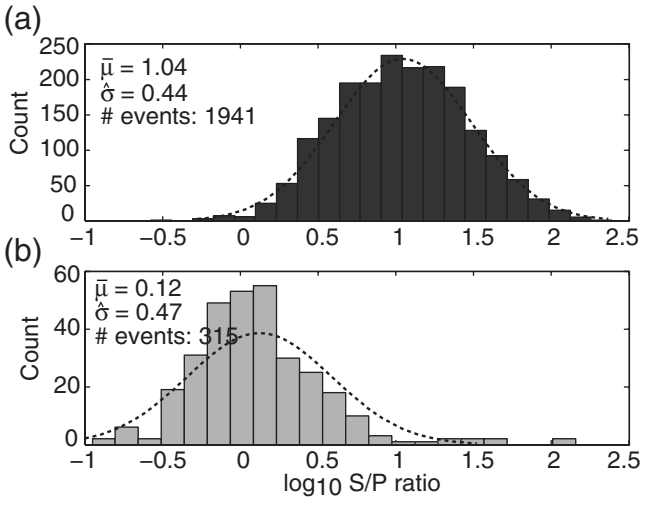

Figure 8. Histograms of S/P amplitude ratios for (a) earthquakes and (b) quarry blasts, including only traces with an epicentral distance of at least 100 km. The difference in mean $\bar{\mu}$ distribution for quarries and earthquakes increases compared to the results at all distances (see Fig. 7).

provided that reliable picks are available. At least in southern California, spectral misfit to an ω^{-2} model is a more reliable discrimination method than the P/S amplitude ratio.

Acknowledgments

We thank Guoqing Lin for relocating all of the events. This research was supported by the Air Force Research Laboratory, Contract Number FA8718-06-C-0004, and by the Southern California Earthquake Center. SCEC is funded by the National Science Foundation (NSF) Cooperative Agreement Number EAR-0106924 and the U.S. Geological Survey (USGS) Cooperative Agreement Number 02HQAG0008. The SCEC contribution number for this article is 1145.

References

Agnew, D. C. (1990). The use of time-of-day seismicity maps for earthquake/explosion discrimination by local networks, with an application to the seismicity of San Diego county, *Bull. Seismol. Soc. Am.* **80,** no. 3, 747–750.

Allmann, B., and P. Shearer (2007). Spatial and temporal stress drop variations in small earthquakes near Parkfield California, *J. Geophys. Res.* **112,** B04305, doi 10.1029/2006JB004395.

Arrowsmith, S. J., M. D. Arrowsmith, M. A. H. Hedlin, and B. Stump (2006). Discrimination of delay-fired mine blasts in Wyoming using an automatic time-frequency discriminant, *Bull. Seismol. Soc. Am.* **96,** no. 6, 2368–2382.

Arrowsmith, S. J., M. A. H. Hedlin, M. D. Arrowsmith, and B. Stump (2007). Identification of delay-fired mining explosions using seismic arrays: application to the PDAR array in Wyoming, USA, *Bull. Seismol. Soc. Am.* **97,** no. 3, 989–1001.

Bennett, T., and J. Murphy (1986). Analysis of seismic discrimination capabilities using regional data from western United States events, *Bull. Seismol. Soc. Am.* **76,** no. 4, 1069–1086.

Brune, J. (1970). Tectonic stress and spectra of seismic shear waves from earthquakes, *J. Geophys. Res.* **75,** 4997–5009.

Carr, D. B., and H. D. Garbin (1998). Discriminating ripple-fired explosions with high-frequency (> 16 Hz) data, *Bull. Seismol. Soc. Am.* **88,** no. 4, 963–972.

Gitterman, Y., and T. van Eck (1993). Spectra of quarry blasts and microearthquakes recorded at local distances in Israel, *Bull. Seismol. Soc. Am.* **96,** no. 4, 129–142.

Gitterman, Y., V. Pinsky, and A. Shapira (1998). Spectral classification methods in monitoring small local events by the Israel seismic network, *J. Seismol.* **2,** no. 2, 237–256.

Hartse, H. E., W. S. Phillips, M. C. Fehler, and L. S. House (1995). Single-station spectral discrimination using coda waves, *Bull. Seismol. Soc. Am.* **85,** no. 5, 1464–1474.

Hauksson, E., and P. Shearer (2005). Southern California hypocenter relocation with waveform cross-correlation; part 1, results using the double-difference method, *Bull. Seismol. Soc. Am.* **95,** no. 3, 896–903.

Hedlin, M. A. (1998). A global test of a time-frequency small-event discriminant, *Bull. Seismol. Soc. Am.* **88,** 973–988.

Hedlin, M. A., J. B. Minster, and J. A. Orcutt (1989). The time-frequency characteristics of quarry blasts and calibration explosions recorded in Kazakhstan, USSR, *Geophys. J. Int.* **99,** no. 1, 109–122.

Hedlin, M. A., J. B. Minster, and J. A. Orcutt (1990). An automatic means to discriminate between earthquakes and quarry blasts, *Bull. Seismol. Soc. Am.* **80,** no. 6B, 2143–2160.

Kim, W. Y., D. W. Simpson, and P. G. Richards (1994). High-frequency spectra of regional phases from earthquakes and chemical explosions, *Bull. Seismol. Soc. Am.* **84,** no. 5, 1365–1386.

Lin, G., P. M. Shearer, and E. Hauksson (2007). Applying a three-dimensional velocity model, waveform cross correlation, and cluster analysis to locate southern California seismicity from 1981 to 2005, *J. Geophys. Res.* **112,** B12309, doi 10.1029/2007JB004986.

Madariaga, R. (1976). Dynamics of an expanding circular fault, *Bull. Seismol. Soc. Am.* **66,** 639–666.

McLaughlin, K. L., J. L. Bonner, and T. Barker (2004). Seismic source mechanisms for quarry blasts: modelling observed Rayleigh and Love wave radiation patterns from a Texas quarry, *Geophys. J. Int.* **156,** no. 1, 79–93.

Plafcan, D., E. Sandvol, D. Seber, M. Barazangi, A. Ibenbrahim, and T.-E. Cherkaoui (1997). Regional discrimination of chemical explosions and earthquakes: A case study in Morocco, *Bull. Seismol. Soc. Am.* **87,** no. 5, 1126–1139.

Prieto, G., P. M. Shearer, F. L. Vernon, and D. Kilb (2004). Earthquake source scaling and self-similarity estimation from stacking *P* and *S* spectra, *J. Geophys. Res.* **109,** B08310, 10.1029/2004JB003084.

Richards-Dinger, K. B., and P. M. Shearer (2000). Earthquake locations in southern California obtained using source-specific stations terms, *J. Geophys. Res.* **105,** no. B5, 10,939–10,960.

Shearer, P., G. Prieto, and E. Hauksson (2006). Comprehensive analysis of earthquake source spectra in southern California, *J. Geophys. Res.* **111,** B06303, doi 10.1029/2005JB003979.

Smith, A. T. (1993). Discrimination of explosions from simultaneous mining blasts, *Bull. Seismol. Soc. Am.* **83,** no. 1, 160–179.

Stump, B. W., M. A. Hedlin, D. C. Pearson, and V. Hsu (2002). Characterization of mining explosions at regional distances: implications with the international monitoring system, *Rev. Geophys.* **40,** no. 4, 1011, doi 10.1029/1998RG000048.

Su, F., K. Aki, and N. N. Biswas (1991). Discriminating quarry blasts from earthquakes using coda waves, *Bull. Seismol. Soc. Am.* **81,** no. 1, 162–178.

Taylor, S. R., N. W. Sherman, and M. D. Denny (1988). Spectral discrimination between NTS explosions and western United States earthquakes at regional distances, *Bull. Seismol. Soc. Am.* **78,** no. 4, 1563–1579.

Walter, W. R., K. M. Mayeda, and H. J. Patton (1995). Phase and spectral ratio discrimination between NTS earthquakes and explosions; part I, empirical observation, *Bull. Seismol. Soc. Am.* **85,** no. 4, 1050–1067.

Warren, L., and P. Shearer (2000). Investigating the frequency dependence of mantle *Q* by stacking *P* and *PP* spectra, *J. Geophys. Res.* **105,** 25,391–25,402.

Warren, L., and P. Shearer (2002). Mapping lateral variations in upper mantle attenuation by stacking *P* and *PP* spectra, *J. Geophys. Res.* **107,** no. B12, 2342, doi 10.1029/2001JB001195.

Wiemer, S., and M. Baer (2000). Mapping and removing quarry blast events from seismicity catalogs, *Bull. Seismol. Soc. Am.* **90,** no. 2, 525–530.

Wuester, J. (1993). Discrimination of chemical explosions and earthquakes in central Europe—a case study, *Bull. Seismol. Soc. Am.* **83,** 1184–1212.

Cecil H. and Ida M. Green Institute of Geophysics and Planetary Physics
Scripps Institution of Oceanography
University of California, San Diego
9500 Gilman Drive
La Jolla, California 92093-0225
ballmann@ucsd.edu
(B.P.A., P.M.S.)

Seismological Laboratory
California Institute of Technology
Pasadena, California 91125
(E.H.)

Manuscript received 24 August 2007